Effective connectivity inferred from fMRI transition dynamics during movie viewing points to a balanced reconfiguration of cortical interactions

Matthieu Gilson[1], Gustavo Deco[1,2], Karl Friston[3], Patric Hagmann[4,5], Dante Mantini[6,7], Viviana Betti[8], Gian Luca Romani[8], Maurizio Corbetta[8,9]

[1]Center for Brain and Cognition, Computational Neuroscience Group, Department of Information and Communication Technologies, Universitat Pompeu Fabra, Roc Boronat 138, Barcelona, 08018, Spain

[2]Institució Catalana de la Recerca i Estudis Avançats (ICREA), Universitat Pompeu Fabra, Passeig Lluís Companys 23, Barcelona, 08010, Spain

[3]Wellcome Trust Centre for Neuroimaging, Institute of Neurology, University College London, 12 Queen Square, London WC1N 3BG, United Kingdom

[4]Department of Radiology, Lausanne University Hospital and University of Lausanne (CHUV-UNIL), Rue du Bugnon 46, 1011 Lausanne, Switzerland

[5]Signal Processing Lab 5, École Polytechnique Fédérale de Lausanne (EPFL), Station 11, 1015 Lausanne, Switzerland

[6]Research Center for Motor Control and Neuroplasticity, KU Leuven, 101 Tervuursevest, 3001 Leuven, Belgium

[7]Department of Health Sciences and Technology, ETH Zurich, Winterthurerstrasse 190, 8057 Zurich, Switzerland

[8]Institute of Advanced Biomedical Technologies - G. d'Annunzio University Foundation, Department of Neuroscience Imaging and Clinical Science, G. d'Annunzio University, Via dei Vestini 31, Chieti, 66013, Italy

[9]Departments of Neurology, Radiology, Anatomy of Neurobiology, School of Medicine, Washington University, St. Louis, St Louis, USA

Corresponding author:
Matthieu Gilson, Universitat Pompeu Fabra, C/ Tanger, 122-140, 08018 Barcelona, Spain
matthieu.gilson@upf.edu

Conflicts of interest: the authors declare no conflict of interest.

ABSTRACT

Our behavior entails a flexible and context-sensitive interplay between brain areas to integrate information according to goal-directed requirements. However, the neural mechanisms governing the entrainment of functionally specialized brain areas remain poorly understood. In particular, the question arises whether observed changes in the activity for different cognitive conditions are explained by modifications of the (intrinsic) inputs or (extrinsic) recurrent connectivity? Here, we show that fMRI transitions over successive time points – a new version of dynamic functional connectivity compared to usual definitions – convey information about the task performed by 19 subjects, namely watching a movie versus a black screen (rest). We use a theoretical framework that extracts this information to characterize the mechanisms underlying cortical coordination at the whole brain level. Our approach relies on our recent network model that was introduced for resting-state fMRI and estimates both the amplitude of input fluctuating activity to each of the 66 cortical regions and the strengths of cortico-cortical interactions between them. In our model, the change of condition does modify the (extrinsic) recurrent connectivity as much as the (intrinsic) inputs, which are putatively related to the movie stimulus. However,, detailed changes in connectivity preserve a balance in the propagation of fluctuating activity and select specific pathways that integrate sensory information from the visual and auditory systems to high-level regions of the brain.. These findings speak to a dynamic functional integration that underlies the hierarchical processing in the brain.

INTRODUCTION

The brain comprises a large number of functionally distinct areas in which information and computational processes are both segregated and integrated (Van Essen et al., 1992; Biswal et al., 1995). A fundamental question in system neuroscience is how information can be processed in a distributed fashion by the neuronal architecture. Brain regions exhibit a high degree of functional diversity, with a massive number of connections that coordinate their activity. Accordingly, empirical evidence from functional magnetic resonance imaging (fMRI), electro-encephalography (EEG), magneto-encephalography (MEG) in humans, as well as cell recordings in animals, supports the notion that brain functions involve multiple brain areas (e.g., Cabeza and Nyberg, 2000). Long-range synchronization of brain activity has been proposed as a dynamical mechanism for mediating the interactions between distant neuronal populations at the cellular level (Engel et al., 2001; Fries, 2005), as well as within large-scale cortical subnetworks both at rest (Grecius et al., 2003; Fox and Raichle, 2007; Brookes et al., 2011; de Pasquale et al., 2012) and when performing a task (Hipp et al., 2011; Betti et al. 2013).

Depending on the task, cortical dynamics reshape the global pattern of correlated activity observed using neuroimaging – or functional connectivity (FC) – as compared to the so-called resting state (de Pasquale et al., 2015; Spadone et al., 2015). Presumably, both sensory-driven and cognitive-driven processes are involved in shaping FC. In particular, the temporal aspect of fMRI signals has been much studied – in relation to tasks performed by subjects – via the concept of 'dynamic FC' (Hutchison et al., 2013), but the usual definition evaluates FC over period of minutes and studies its fluctuations over time. At the timescale of successive TRs, it has recently been demonstrated that transitions in fMRI activity convey information about the behavioral states (Mitra et al. 2015). However, it remains unclear how to extract this functionally relevant information in those measurements and relate them to the underlying cortical coordination.

In this paper, we examine the specific role played by long-range neuro-anatomical projections between brain areas in shaping the intracortical communication, resulting in the measured FC. We rely on the well-established hypothesis that both the activity and coordination of different regions depend on both the local activity and intracortical connectivity (Stephan et al., 2004). Based on dynamic models for blood oxygen level dependent (BOLD) activity at the level of a cortical region, techniques have been developed to estimate the connectivity strengths: the notion of 'effective connectivity' (EC) describes causal pairwise interactions at the network level (McIntosh and Gonzalez-Lima, 1994; Friston, 2002; Honey et al., 2007; Friston and Dolan, 2010; Deco et al., 2011; Cabral et al., 2011). The distinction between functional and effective connectivities is crucial here: FC is defined as the statistical dependence between distant neuro-physiological activities, whereas EC is defined as the influence one neural system exerts over another (Friston et al., 2003). In neurophysiology, EC was originally defined as the simplest

circuit diagram that could replicate observed patterns of functional connectivity (Aertsen et al., 1989).

Here, we use a noise-diffusion network model (or multivariate Ornstein-Uhlenbeck process) to capture spatiotemporal information in FC, namely, BOLD covariances with and without time shifts. EC is the directed network connectivity that governs the propagation of the fluctuating activity that generates FC at the global level. Both EC and region-specific input variability – respectively extrinsic and intrinsic to the local neuronal population of each ROI – are inferred using a recently proposed method (Gilson et al., 2016); the present paper is the first application to task-evoked fMRI data. The integration of anatomical data obtained from diffusion spectrum imaging (DSI) is crucial to constrain EC. The network estimates then provide a mechanistic explanation for the information propagation and integration in the brain observed via the fMRI data.

MATERIAL AND METHODS

Study design for Empirical fMRI data during Resting and Passive Movie Viewing:

We re-analyzed BOLD imaging data reported in our previous papers (Hlinka et al., 2011; Mantini et al., 2012; Mantini et al., 2013). Twenty-four right-handed young, healthy volunteers (15 females, 20–31 years old) participated in the study. They were informed about the experimental procedures, which were approved by the Ethics Committee of the Chieti University, and signed a written informed consent. The study included a resting state with eyes opened and a natural viewing condition. In the resting state, participants fixated a red target with a diameter of 0.3 visual degrees on a black screen. In the natural viewing condition, subjects watched (and listened) to 30 minutes of the movie 'The Good, the Bad and the Ugly' in a window of 24x10.2 visual degrees. Visual stimuli were projected on a translucent screen using an LCD projector, and viewed by the participants through a mirror tilted by 45 degrees. Auditory stimuli were delivered using MR-compatible headphones.

Data acquisition:

Functional imaging was performed with a 3T MR scanner (Achieva; Philips Medical Systems, Best, The Netherlands) at the Institute for Advanced Biomedical Technologies in Chieti, Italy. The functional images were obtained using T2*-weighted echo-planar images (EPI) with BOLD contrast using SENSE imaging. EPIs comprised of 32 axial slices acquired in ascending order and covering the entire brain (230 x 230 in-plane matrix, TR/TE=2000/35, flip angle = 90°, voxel size=2.875×2.875×3.5 mm3). For each subject, 2 and 3 scanning runs of 10 minutes duration were acquired for resting state and natural viewing, respectively. Only the first 2 scans are used here, to have the same number of time points for the two conditions. Each run included 5 dummy volumes – allowing the MRI signal to reach steady state and an additional 300 functional volumes that were used for analysis. Eye position was monitored during scanning using a pupil-corneal reflection system at 120 Hz (Iscan, Burlington, MA, USA). A three-dimensional high-resolution T1-weighted image, for anatomical reference, was acquired using an MP-RAGE sequence (TR/TE=8.1/3.7, voxel size=0.938x0.938x1 mm3) at the end of the scanning session.

Data processing:

Data were preprocessed using SPM8 (Wellcome Department of Cognitive Neurology, London, UK) running under MATLAB (The Mathworks, Natick, MA). The preprocessing steps involved: (1) correction for slice-timing differences (2) correction of head-motion across functional images, (3) coregistration of the anatomical image and the mean functional image, and (4) spatial normalization of all images to a standard stereotaxic space (Montreal Neurological Institute, MNI) with a voxel size of 3×3×3 mm^3. Furthermore, the BOLD time series in MNI space were subjected to spatial independent component analysis (ICA) for the identification and removal of artifacts

related to blood pulsation, head movement and instrumental spikes (Sui et al., 2009). This BOLD artifact removal procedure was performed by means of the GIFT toolbox (Medical Image Analysis Lab, University of New Mexico). No global signal regression or spatial smoothing was applied.

For each recording session (subject and run), we extracted the mean BOLD time series from the 66 regions of interest (ROIs) of the brain atlas used in Hagmann et al. (2008); see Table 1 for details. For each ROI, we calculated the overall percent signal change value in the natural viewing condition using the resting state condition as baseline. For resting state and natural viewing sessions separately, we concatenated the BOLD time series for each region, and calculated the 66x66 correlation matrix representing the FC between each pair of cortical areas.

Structural Connectivity Matrix:

Anatomical connectivity was estimated from Diffusion Spectrum Imaging (DSI) data collected in five healthy right-handed male participants (Hagmann et al., 2008; Honey et al., 2009). The gray matter was first parcellated into 66 ROIs, using the same low-resolution atlas used for the FC analysis (Hagmann et al., 2008). For each subject, we performed white matter tractography between pairs of cortical areas to estimate a neuro-anatomical connectivity matrix. In our method, the DSI values are only used to determine the skeleton: a binary matrix of structural connectivity (SC) obtained by averaging the matrices over subjects and applying a threshold for the existence of connections. The strengths of individual intracortical connections do not come from DSI values, but are optimized as explained below.

It is known that DSI underestimates inter-hemispheric connections (Hagmann et al., 2008). Homotopic connections between mirrored left and right ROIS are important in order to model whole-cortex BOLD activity (Messé et al. 2014). Therefore we add for all ROIs homotopic connections, which are also tuned during the optimization. This increases the density of structural connectivity (SC) from 27% to 28%.

Empirical covariances:

For each of the two sessions of 10 minutes for rest and movie, the BOLD time series s_i^t for each region $1 \le i \le N$ with time indexed by $1 \le t \le T$ (T=300 time points separated by a TR=2 seconds). Each time series s_i^t is centered to remove the mean signal. Following Gilson et al. (2016), the empirical covariances are calculated as:

$$\hat{Q}_{ij}^0 = \frac{1}{T-1} \sum_{1 \le t \le T} s_i^t s_j^t \quad \text{and} \quad \hat{Q}_{ij}^1 = \frac{1}{T-2} \sum_{1 \le t \le T-1} s_i^t s_j^{t+1} . \qquad (1)$$

For each individual and session, we calculate the time constant τ_x associated with the exponential decay of the autocovariance function $\hat{Q}_{ii}^{\tau}$ averaged over all regions:

$$\tau_x = \frac{1}{N}\sum_i \frac{1}{\log\left(\hat{Q}_{ii}^0\right) - \log\left(\hat{Q}_{ii}^1\right)}. \quad (2)$$

This is used to calibrate the model, which is subsequently optimized to reproduce the empirical covariances. Similar calculations are done for $\tau = 2$ TR.

Dynamic cortical model:

The model comprised $N = 66$ interconnected cortical regions, each of them receiving a noisy input. The resulting fluctuating activity is shaped by the recurrent effective connectivity C to generate the functional connectivity embodied in the matrix Q. More precisely, the network model is a multivariate Ornstein-Uhlenbeck process, where each node (indexed by $1 \le i \le N$) has an activity variable x_i that decays exponentially with time constant τ_x (estimated using Eq. 2) and evolves depending on the activity of other populations: $\frac{dx_i}{dt} = \frac{-x_i}{\tau_x} + \sum_{j \ne i} C_{ij} x_j + dB_i$. Here, dB_i is colored Gaussian noise with covariance matrix Σ, with the variances of the random fluctuations on the diagonal and off-diagonal elements corresponding to input cross-correlations. In practice, we only consider input cross-correlations for homotopic regions in the visual and auditory ROIs: CUN, PCAL, LING, LOCC, ST, TT and MT (see Table 1). The extrinsic (between-region) effective connectivity is encoded by the matrix C, for which DSI determines the skeleton (see details above). In our model, all variables x_i have zero mean and their spatiotemporal covariances arise from the noisy inputs dB_i; they are defined as $Q_{ij}^\tau = \left\langle x_i^t x_j^{t+\tau} \right\rangle$, where the angular brackets denote averaging over random fluctuations. In practice, we use two time shifts: $\tau = 0$ on the one hand and $\tau = 1$ or 2 TR on the other hand, as this is sufficient to characterize the network parameters.

The matrices C and Q^0 are related via a Lyapunov equation: $JQ^0 + Q^0 J^T + \Sigma = 0$, where the Jacobian of the dynamical system $J_{ij} = -\delta_{ij}/\tau_x + C_{ij}$ depends on the mean activity of the network; the superscript *T* denotes the matrix transpose and δ_{ij} is the Kronecker delta. The time shifted covariance for any $\tau > 0$ is given by $Q^\tau = Q^0 \mathrm{expm}(J^T \tau)$, where expm denotes the matrix exponential. These two consistency equations allow for the quick estimation of the predicted FC matrices, without simulating the network.

Parameter estimation procedure:

We tune the model such that its covariance matrices Q^0 and Q^τ reproduce the empirical FC, namely $\hat{Q}^0$ and $\hat{Q}^\tau$, with τ being either 1 or 2 TR. We summarize the essential steps of the

procedure described in Gilson et al. (2016) that iteratively optimizes the network parameters C and Σ. At each step, the Jacobian J is calculated from the current value of C. Then, the model FC matrices Q^0 and Q^τ are calculated from the consistency equations, using the Bartels-Stewart algorithm to solve the Lyapunov equation. The desired Jacobian update is the matrix $\delta J^T = \left(Q^0\right)^{-1}\left[\delta Q^0 + \delta Q^1 \mathrm{expm}\left(-\mathrm{J}^\mathrm{T}\tau\right)\right]$, which involves the FC error between the empirical and model matrices, namely $\delta Q^0 = \hat{Q}^0 - Q^0$ and $\delta Q^\tau = \hat{Q}^\tau - Q^\tau$. Finally, the connectivity update is $\delta C_{ij} = \eta_C \delta J_{ij}$ for existing connections. We impose non-negativity of the EC values during the optimization. The input variances are tuned according to $\delta\Sigma_{ii} = -\eta_\Sigma\left(J\delta Q^0_{ii} + \delta Q^0_{ii} J^T\right)$. We use $\eta_C = 0.0001$ and $\eta_\Sigma = 0.1$.

Normalized statistical scores and effective drive (ED):

We define the following z-scores for *X* being a matrix element C_{ij} and Σ_{ij} – for the whole distribution over all connections and subjects – as

$$\mathrm{score}(\mathrm{X}) = \frac{\mathrm{mean}(X) - l_X}{\mathrm{std}(X)}, \qquad (3)$$

where l_X is the median of the corresponding distribution illustrated by the dashed-dotted line in Fig. 6A.

We also define the effective drive as

$$\mathrm{ED}_{\mathrm{ij}} = \mathrm{score}(C_{\mathrm{ij}}\sqrt{Q^0{}_{jj}}), \qquad (4)$$

with the corresponding median l_{ED}. It measures how the fluctuating activity at region j with standard deviation $\sqrt{Q^0{}_{jj}}$ propagates to region i.

Non-parametric bootstrap method for significance test

From the individual estimates for the two conditions, we calculate the two means and we compare them with a null distribution comprising of generating 1000 surrogate means obtained when mixing the condition labels for each subject. Then we test – for each element C_{ij} or Σ_{ij} – whether the rest and movie means are in the 0.1% tails of the null distribution (in opposite tails).

RESULTS

1. Changes in FC induced by movie viewing

We analyze BOLD signals recorded in 19 healthy volunteers recorded when watching either a black screen – referred to as rest – or a movie (2 sessions of 10 minutes for each condition). These signals are aggregated according to the parcellation of 66 cortical regions – or regions of interest (ROIs) – that are listed in Table 1. Firstly, we examine changes in their spatiotemporal covariances between the two conditions, as these functional observables to feed the dynamic cortical model (Gilson et al., 2016). Doing so, we also address the question of how to extract information from the BOLD time series that is relevant to discriminate between two viewing conditions. As shown in Fig. 1A, the BOLD signals do not exhibit large changes in their mean between the conditions (each cross represents a ROI), but the BOLD variances is significantly modified for some ROIs (blue crosses). Now averaging those values over all ROIs for each individual, we observe in all subjects larger variances for the movie than for rest (squares), unlike BOLD means (circles); the black lines in Fig. 1B indicate a perfect match.

The right panel of Fig. 1B displays time constants τ_x (triangles) estimated from BOLD autocovariance functions. They indicate the "memory depth" of corresponding time series; namely, how much the BOLD activity at a given TR influences the successive TRs (see Eq. 2 in Methods). Here, we assume a single time constant for all ROIs per condition; at this level, no consistent change is observed between the two conditions. From the two plots in Fig. 1B, we discard three individuals (in red) with extreme values: two for the variances (large variance for movie) and one for the time constant (small values for both conditions). From the original 22 subjects, this leaves 19 for subsequent analysis, for which we calculate the FC along all ROIs: in our framework, FC0 corresponds to an instantaneous covariance (with no time shifts), whereas FC1 corresponds to a life of one repetition time (TR); see Eq. 1 in Methods where FC matrices are denoted by Q. We evaluate the significance of changes for each matrix element using Welch's t-test. As shown in Fig. 1C (in order of the smallest p-values): changes in BOLD variances principally concern the early visual and auditory pathways (rLOCC, lLOCC, rCUN, lCUN, rST, lST, lMT), as well as multimodal integration regions (rFUS, lFUS, rBSTS, lBSTS, rIP, lIP); in addition, we find changes for lPORB in the frontal lobe and the two central regions rPARH and lENT. Fig. 1D displays the significance for all matrix elements of FC0 and FC1.

Many studies of resting state BOLD activity focused on correlations (Deco et al., 2011; Messé et al. 2014), which can be considered as "spatial" FC. Fig. 1E shows that correlations also convey significant information about the two conditions (to be compared with Fig. 1D), which is confirmed by the black cumulative histogram in Fig. 1F. However, variances are proportionally more informative for discriminating between the two conditions, which supports our approach that does not mix variances and covariances in correlations, but use them fully. Moreover, FC1 also

convey a small number of significant elements (green curve).

2. A noise-diffusion network model to interpret spatiotemporal FC

In order to interpret the mixed increases and decreases observed in the spatiotemporal FC, we use a dynamic model of the BOLD activity. This generative model is schematically represented in Fig. 2, for a few cortical regions. The skeleton of the network connectivity in Fig. 2A is determined by thresholding the DSI data, which estimate the density of white matter fibers between the 66 ROIs; gray pixels indicate homotopic connections that are added post-hoc, as described in Methods. Note that we only retain information about the existence of connections and discard quantitative details of the DSI values. Importantly, the matrix C in Fig. 2B (representing EC) is in general not symmetric, as illustrated by the uneven red arrows in the schematic diagrams. In our model, each ROI receives a fluctuating input that propagates via the recurrent EC. The covariances of the resulting network activity give the model FC at the global level, which thus depends on both C and the input covariances Σ.

The network parameters are estimated from the empirical data using an iterative optimization that tunes the model such as to best reproduce empirical FC matrices, as represented in Fig. 2C. The model is initially calibrated by the estimated time constants τ_x in Fig. 1B, one value for all ROIs per each subject and condition. As demonstrated in Gilson et al. (2016), both C and Σ must be estimated in order to extract unambiguously the spatiotemporal information in FC0 and FC1. The uniqueness of this estimation follows from the bijective mapping from the model parameters C and Σ to the FC pair (FC0,FC1). Importantly, the estimated value for each individual weight depends on all others: the method is designed to capture the network effects due to the recurrent feedback; in particular, the resulting C matrix is asymmetric in general and the directionality is strongly related to the time-shifted FC1. The precision of the estimated parameters is limited by the number of time points in the BOLD signals, as with all models.

The goodness of fit for each subject and condition is satisfactory: an example of correspondence for FC0 is illustrated in Fig. 3A (left panel). The Pearson correlation between the model and empirical FC matrices elements is larger than 0.7 for almost all subjects and conditions – synonymous with high accuracy – as summarized in the right panel of Fig. 3A. Importantly, the model captures the change in FC between the two conditions, as illustrated in the right panels of Fig. 3B in similar plots to Fig. 3A; the Pearson correlation between the model and empirical ΔFC (movie minus rest) is larger than 0.6 for most subjects. The parametric p-values for the changes in FC0 matrix elements are in good agreement with their empirical counterparts in Fig. 3C, with a Pearson correlation coefficient of 0.8 with $p<10^{-10}$. Only elements corresponding to absent EC connections (in black) are not in good agreement; correcting SC with the addition of missing edges would improve this aspect, but this requires more DSI data. To further verify the robustness of estimated parameters, we repeat the same estimation procedure using FC0 and FC2, that is, a

time shift of 2 TR instead of 1 TR. We found nearly identical Σ estimates and very similar C estimates (see Fig. 3D), in a similar manner to our previous results for resting-state data (Gilson et al., 2016).

To characterize the respective effect of the model parameters, we relate them to the FC observables. As shown in Fig. 3E (left panel), $\Delta\Sigma$ is closely related to the change in empirical BOLD variances: the model M/R (in red) that combines C from the movie condition and Σ from rest reproduces the FC during movie viewing much more poorly than M/M (in blue), which is the model estimated from the movie data. In contrast, ΔC rather reflects the changes in FC0 covariances (off-diagonal) and FC1, as indicated by the comparison between the model R/M (in green) and M/M (in blue) reported in the middle and right panels. As can be understood from the Lyapunov equation (based on our analysis of the noise-diffusion model in Methods), changes in FC0 alone cannot disentangle the contributions from inputs and connectivity. Our approach resolves this indeterminacy by considering both FC0 and FC1 (or FC2).

3. Estimation of cross-input correlations

A specific aspect of the model optimization concerns cross-correlated inputs, embodied in the non-diagonal elements of Σ. This feature represents ROIs that receive common information via their inputs. We restrict our study to the comparison between the absence of cross-correlations and their presence for 7 pairs of homotopic visual and auditory ROIs (both left and right CUN, PCAL, LING, LOCC, ST, TT, MT); their actual values are estimated in the same manner as the input variances during the optimization. Performing the estimation procedure for both models, we evaluate in Fig. 4A the significance of the changes in Σ, which is measured by Welch's t-test as in Fig. 1C. Many changes concern cross-correlated inputs ('x') when they are present, suggesting that they are important to model.

Another important point is that the ranking – which is similar for both models for common input elements – significantly differs from that in Fig. 1B. This means that the changes observed in the model BOLD variances are not solely related to their individual inputs - for example, the increase in the variance of rIP in Fig. 1C does not come from the corresponding Σ value. Instead, our model captures network effects to collectively explain the changes for all ROIs.

In Fig. 4B, the between-hemisphere and inter-hemisphere parameters are grouped together (circles and triangles, respectively) in order to compare the two models. In particular, it examines how these estimates explain the increase of empirical FC - from rest to movie, as measured by the log ratio on the y-axis – observed with equal magnitude within and between hemispheres. The model without cross-correlated inputs (in black) slightly overestimates the increase in inter-hemispheric connectivity compared to the model with them (in red). Apart from that, both models give similar changes in parameters. This confirms that the model inputs should be properly

defined based on further anatomical knowledge for existing common inputs. For simplicity, we only consider such inputs for sensory ROIs involved in the task here.

4. Movie viewing induces greater changes in (intrinsic) activity than (extrinsic) connectivity

We now analyze the differences of the estimated parameters between rest and movie at the whole network level. The power of our model-based approach is to disambiguate intrinsic from extrinsic causes, following previous studies on effective connectivity (Friston et al. 2003; Battaglia et al., 2012). The distribution of Σ – over all subjects and relevant matrix elements – is more affected than that of C, as shown in Fig. 5A. Moreover, these changes are also more significant, as represented in Fig. 5B by the cumulative histograms of the -log(p-value) corresponding to the parametric t-test for each C and Σ matrix element (in a similar manner to Fig. 1 D). Changes with p-value<0.01 (uncorrected) for Σ identify 9 ROIs out of 66 (14%) and 3 inter-hemispheric correlated inputs out of 7 (43%), whereas only 87 connections out of 1180 (7%) are concerned for C. In summary, changes in intrinsic inputs are stronger both in magnitude and in significance.

5. Sensory integration in the visual and auditory cortical systems

Now we turn to a detailed analysis of the ROIs where the changes in Σ occur, which are located in the occipital and temporal regions as illustrated in Fig. 6A. The ROIs with most significant changes (from Figs. 4A and 5B) concern visual and auditory ROIs. To further characterize the significance of the changes in both C and Σ, we perform a non-parametric significance test based on bootstrap (see Methods for details): for each matrix elements, we build a null distribution making surrogates for the mean value over the subjects by mixing the rest and movie labels. With p-value<0.001 (uncorrected), we find increases of diagonal Σ values for 10 out of 14 ROIs in the early visual and auditory pathways (both LOCC, PCAL, ST, MT as well as rCUN and lIT). Moreover, correlated inputs to LOCC, PCAL, ST, MT increases as well. We explain this increased intrinsic activity by a larger stimulus load to those ROIs for movie than rest. We also find an increase of Σ for 6 ROIs related to multimodal integration: FUS, TP and IP from both hemispheres. Last, 7 other ROIs exhibit similar increases for Σ: both ENT and PSTC, as well as rMOF, rPARH and lPORB. On the EC side, 25 changes in C involve visual and auditory ROIs, versus 9 that do not.

Together, these parametric and non-parametric statistical analyses point at visual, auditory and integration ROIs. We thus focus on those subsystems, whose anatomical SC is represented in Fig. 6B. This dense connectivity exhibits a hierarchy, represented along the diagonal, from sensory ROIs – at each end, visual in the bottom left and auditory in the top right – toward the integration regions in the middle – FUS and BSTS. To estimate the changes over the pool of subjects, we define normalized statistical z-scores for C and Σ elements, as illustrated in Fig. 6C; these scores evaluate the probability of large values for each matrix element with respect to the

histograms in Fig. 5A (the median used in the definition is indicated by the dashed line, see Eq. 3 in Methods). As expected from Fig.5, changes in Σ scores are larger than those in C.

6. Dynamical balance in the integration of sensory inputs

In order to make sense of the smaller and diverse (both positive and negative) changes in C, we define the 'effective drive' (ED): it measures – for each connection – to which extent the local fluctuating activity (i.e., standard deviation of BOLD signal) of the source ROI is transferred to the target ROI, as illustrated in Fig. 7A. For the noise-diffusion network, ED is a canonical measure for the propagation of fluctuations. We further define a statistical z-score for ED similar to that for Σ and C; see Eq. (4) in Methods. In Fig. 7A, ED clearly shows the hierarchical processing from visual and auditory ROIs to the associative or integrative ROIs (FUS and BSTS). Importantly, this bimodal information integration is enhanced when watching a movie compared to a black screen. The difference ΔED between the effective drive in movie and rest is shown in the middle panel of Fig. 7B: most increases concern diagonal elements and, interestingly, the z-scores of ED for many feedback connections from the integration ROIs are larger in the movie condition, in particular from FUS to CUN and LING, as well as from BSTS to TT.

Thanks to our model-based approach, we can decompose the contributions of inputs and connectivity in ΔED: if only inputs are modified ($\Delta\Sigma$), the whole area saturates with high activity and the integrative ROIs are no longer driven by the sensory inputs. The changes in C regulate this sensory drive and boost the connections from the integrative FUS and BSTS to LOCC and ST. In other words, $\Delta\Sigma$ can be related to the stimulus load in our model and its propagation is gated or modulated along specific pathways by ΔC. Strikingly, the effects of $\Delta\Sigma$ and ΔC in Fig. 7B oppose each other, suggesting a dynamic balance of the cortical information flow across conditions.

7. Path selection in the cortical network

Now we step back to the whole cortex and analyze the changes in ED for all ROIs grouped into 6 functional ensembles: in addition to the visual, auditory and integration regions examined in Figs. 6 and 7, we examine motor, frontal and central regions; see the table in Fig. 8A. These groups are defined for illustration purpose and do not follow strict functional categorization. At the global level, ED exhibits an increase of forward interactions from the visual and auditory groups to the integration, frontal and central areas. A moderate increase of feedback from integration to the visual system can also be observed.

However, the global view in Fig. 8A may conceal detailed changes in specific pathways. To analyze the network propagation in more depth, we use the Louvain method (Blondel et al., 2008) on the ED matrix in both conditions to cluster ROIs: in Fig. 8B, darker pixels indicate a participation index in the same cluster for each pair of ROIs. When watching the black screen, we observe that the visual regions are strongly bound together with a few central ROIs; meanwhile,

the auditory group is strongly clustered with the integration, motor and frontal groups. In the movie condition, the integration group splits such that some ROIs cluster with the visual group (as well as central ROIs in green), while the others remain functionally linked to the auditory ROIs. This is another important finding: the two hemispheres are more dynamically connected – as measured by ED – for movie than rest. This especially concerns the participation index of the integration and frontal ROIs (purple and cyan), which are linked to the movie and auditory groups, respectively. Similar results were obtained when applying the Louvain method to the connectivity matrix *C*, instead of ED. This underlines a selective coordination of cortical paths to implement a distributed processing of information.

DISCUSSION

Our results shed light on a fundamental question in neuroscience: how do inputs and connectivity locally interact to generate large-scale integration of information in the brain? To address this question, we use a recently developed model-based approach to interpret functional connectivity, which is the whole-cortex pattern of correlated activity; the present work is the first application to task-evoked activity. The proposed generative model provides quantitative estimates of (extrinsic) effective connectivity and (intrinsic) local excitability. Their combination shapes the information flow in the recurrent cortical network, resulting in FC. In essence, the model allows for the interpretation of cortical communication from task-evoked BOLD time series.

A major finding concerns the reorganization of the extrinsic connectivity during movie viewing, namely how EC is adjusted to select specific pathways for the integration of information. Locally in the auditory and visual systems, it includes a down-regulation of forward connections in a compensatory manner, such that regional inputs do not saturate the network; meanwhile, some specific backward connections are boosted to enable the efficient transmission of top-down signals to sensory areas, despite their activity increases (Fig. 7B). The dynamic balance is expected to be task dependent – in particular in regard of stimulus-related inputs – and speaks to functional synchronization at the network level (changes in BOLD variances in Fig. 1). Our results are in line with previous studies that observed such balanced activity from the neuronal level (Destexhe et al., 2003; Dehghani et al., 2016) to the cortical level (Deco and Corbetta, 2011).

Although the connectivity matrices corresponding to the rest and movie conditions may appear rather similar in structure (Figs. 5A and 6C), their details induce dynamics that lead to a different community pooling (Fig. 8B). At the global level, we observe that homotopic areas increase their information exchange via inter-hemispheric connections (especially parietal and frontal areas), when watching the movie. Note that the model should be extended to incorporate subcortical areas in order to further analyze this inter-hemispheric integration; for example, many correlated inputs to cortical regions may originate from the thalamus. Nevertheless, our model illustrates how the cortex becomes specialized when engaging a task, while specific high-level ROIs remains rather stable and perform global integration by binding the whole cortex (a few parietal and central ROIs in Fig. 8B). This illustrates an elaborate scheme of functional segregation and integration, which is dynamically regulated, but supported by the same structural network (Battaglia et al., 2012).

Beyond the task analyzed here, our study demonstrates that spatiotemporal BOLD (co)variances convey important information about the cognitive state of subjects. This version of dynamics FC corresponds to transitions of fMRI activity between successive TRs; this statistics is averaged over the whole recording period, in contrast to other time-dependent measures such as inter-subject correlations (Hasson et al., 2004), metastability (Deco et al., 2011) or measures of dynamic FC averaged over minutes, corresponding to periods of more than 30 TRs (Hutchinson et

al., 2013). This was already suggested by our previous analysis of resting state (Gilson et al., 2016) and is in line with recent results that focused on the temporal component of BOLD signals (Mitra et al., 2015). Moving beyond the analysis of spatial FC, namely covariances without time shift (FC0) or BOLD correlations, is thus a crucial step toward a better interpretation of fMRI measurements. The advantage of our optimization method compared to multivariate auto-regressive models lies in incorporating information from DSI, which enhances the robustness of the estimation, or constraints on the parameters (non-negativity for C, selected non-zero elements for Σ). Importantly, our approach based on EC for the whole cortex allows us to move from a structure-centric (Cordes et al., 2000) to a network-specific analysis. This offers a new perspective on the interpretation fMRI data: as the amplitudes of BOLD fluctuations (i.e., variances) are informative about the task – and appear consistent with neural computations performed by the cortical areas – the amplitude of region-specific fluctuating inputs determine the local dynamical regime in the proposed model.

The study of neuronal dynamics over the whole cortex is the key to understand the distributed processing of information, as it bridges structure to function. The notion of effective connectivity – as a fingerprint for the dynamical state of the cortex – developed in the present framework is related to the approach of dynamic causal modeling, in the sense that statistical dependences of the ROIs' activities also depend on the input variables (Σ). The results in Fig. 4D show that inputs must be estimated as well as effective connectivity, to explain observed changes in FC0. As shown in Fig. 1, lagged covariances FC1 convey crucial information that discriminates between the states of functional integration. Importantly, the noise in the proposed model is "functional", as the input variances in Σ represent spontaneous activity or can be related to the stimulus load for sensory areas. The focus on the fluctuating activity with the second-order statistics of the BOLD signals changes the perspective and allows for the interpretation of the model estimates in terms of cortical communication. The 'effective drive' in Fig. 7 is tied to the noise-diffusion model and measures the propagation of fluctuations in the network, like an entrainment degree between ROIs. Schematically, we see the BOLD variance as a proxy for the neuronal computation processing at each ROI, while the information flow between ROIs is governed by EC and measured by FC covariances. Unlike dynamic causal modeling (DCM), we do not model intrinsic (self) connectivity, but directly estimate the amplitude of random fluctuations within each region. There is a formal relationship between the estimation of EC describing this paper and DCM for cross spectral density in fMRI. Technically, they both estimate the parameters of a linearized dynamical system under the assumption it is perturbed by random fluctuations with a known spectral density or autocovariance function. The current formulation assumes a simple (Wiener) form for the input fluctuations, which allows for considering a larger number of ROIs than usual applications of DCM. Further comparison is left for subsequent work.

ACKNOWLEDGMENTS

This work was supported by the Human Brain Project (grant FP7-FET-ICT-604102 and H2020-720270 HBP SGA1 to MG and GD) and the Marie Sklodowska-Curie Action (grant H2020-MSCA-656547 to MG). This work was partly supported by the 7th Framework Programme of the European Commission (grant PCIG12-334039 to DM) and the KU Leuven Special Research Fund (grant C16/15/070 to DM). VB was supported by a Post-Doctoral Fellowship grant from the University of Chieti.

REFERENCES

Aertsen AM, Gerstein GL, Habib MK, Palm G (1989) Dynamics of neuronal firing correlation: modulation of “effective connectivity”. J Neurophysiol, 61: 900-917

Battaglia D, Witt A, Wolf F, Geisel T (2012) Dynamic effective connectivity of inter-areal brain circuits. PLoS Comp Biol, 8: e1002438

Betti V, Della Penna S, de Pasquale F, Mantini D, Marzetti L, Romani GL, Corbetta M (2013) Natural scenes viewing alters the dynamics of functional connectivity in the human brain. Neuron, 79: 782-797

Biswal B, Yetkin F, Haughton V, Hyde J (1995) Functional connectivity in the motor cortex of resting human brain using echo-planar MRI. Magn Reson Med, 34: 537-541

Blondel VD, Guillaume J-L, Lambiotte R, Lefebvre E (2008) Fast unfolding of communities in large networks. J Stat Mech, 10: P10008

Brookes MJ, Woolrich M, Luckhoo H, Price D, Hale JR, Stephenson MC, Barnes GR, Smith SM, Morris PG (2011) Investigating the electrophysiological basis of resting state networks using magnetoencephalography. Proc Natl Acad Sci USA, 108: 16783-16788

Cabeza R, Nyberg L (2000) Imaging cognition II: empirical review of 275 PET and fMRI studies. J Cogn Neurosci, 12: 1-47

Cabral J, Hugues E, Sporns O, Deco G (2011) Role of local network oscillations in resting-state functional connectivity. Neuroimage, 57: 130-139

Cordes D, Haughton VM, Arfanakis K, Wendt GJ, Turski PA, Moritz CH, Quigley MA, Meyerand ME (2000) Mapping functionally related regions of brain with functional connectivity MR imaging. AJNR Am J Neuroradiol, 21: 1636-1644

de Pasquale F, Della Penna S, Snyder AZ, Marzetti L, Pizzella V, Romani GL, Corbetta M (2012) A cortical core for dynamic integration of functional networks in the resting human brain. Neuron, 74: 753-764

de Pasquale F, Della Penna S, Sporns O, Romani GL, Corbetta M (2015) A Dynamic Core Network and Global Efficiency in the Resting Human Brain. Cereb Cortex, 26: 4015-4033

Deco G, Corbetta M (2011) The dynamical balance of the brain at rest. Neuroscientist, 17: 107-123

Deco G, Jirsa V, McIntosh A (2011) Emerging concepts for the dynamical organization of resting-state activity in the brain. Nat Rev Neurosci, 12: 43-56

Dehghani N, Peyrache A, Telenczuk B, Quyen MLV, Halgren E, Cash SS, Hatsopoulos NG, Destexhe A (2016) Dynamic Balance of Excitation and Inhibition in Human and Monkey Neocortex. Sci Rep, 6: 23176

Destexhe A, Rudolph M, Pare D (2003) The high-conductance state of neocortical neurons in vivo. Nat Rev Neurosci, 4: 739–751

Engel A, Fries P, Singer W (2001) Dynamic predictions: oscillations and synchrony in top-down processing. Nat Rev Neurosci, 2: 704-716

Fox M, Raichle M (2007) Spontaneous fluctuations in brain activity observed with functional magnetic resonance imaging. Nat Rev Neurosci, 8: 700-711

Fries P (2005) A mechanism for cognitive dynamics: Neuronal communication through neuronal coherence. Trends Cogn Sci, 9: 474-480

Friston K (2002) Beyond phrenology: what can neuroimaging tell us about distributed circuitry? Annu Rev Neurosci, 25: 221-250

Friston K, Harrison L, Penny W (2003) Dynamic causal modelling. Neuroimage, 19: 1273-1302

Friston K, Dolan R (2010) Computational and dynamic models in neuroimaging. Neuroimage, 52: 752-765

Gilson M, Moreno-Bote R, Ponce-Alvarez A, Ritter P, Deco G (2016) Estimation of Directed Effective Connectivity from fMRI Functional Connectivity Hints at Asymmetries of Cortical Connectome. PLoS Comput Biol, 12: e1004762

Greicius MD, Krasnow B, Reiss A, Menon V (2003) Functional connectivity in the resting brain: a network analysis of the default mode hypothesis. Proc Natl Acad Sci USA, 100: 253-258

Hagmann P, Cammoun L, Gigandet X, Meuli R, Honey CJ, Wedeen VJ, Sporns O (2008) Mapping the structural core of human cerebral cortex. PLoS Biol, 6: e159

Hasson U, Nir Y, Levy I, Fuhrmann G, Malach R (2004) Intersubject synchronization of cortical activity during natural vision. Science 303: 1634–1640

Hipp JF, Engel AK, Siegel M (2011) Oscillatory synchronization in large-scale cortical networks predicts perception. Neuron, 69: 387-396

Hlinka J, Palus M, Vejmelka M, Mantini D, Corbetta M (2011) Functional connectivity in resting-state fMRI: is linear correlation sufficient? Neuroimage, 54: 2218-2225

Honey CJ, Kötter R, Breakspear M, Sporns O (2007) Network structure of cerebral cortex shapes functional connectivity on multiple time scales. Proc Natl Acad Sci USA, 104: 10240-10245

Hutchison RM, Womelsdorf T, Allen EA, Bandettini PA, Calhoun VD, Corbetta M, Della Penna S, Duyn JH, Glover GH, Gonzalez-Castillo J, Handwerker DA, Keilholz S, Kiviniemi V, Leopold D A, De Pasquale F, Sporns O, Walter M, Chang C (2013) Dynamic functional connectivity: Promise, issues, and interpretations. Neuroimage, 80: 360–378

Mantini D, Hasson U, Betti V, Perrucci MG, Romani GL, Corbetta M, Orban GA, Vanduffel W (2012) Interspecies activity correlations reveal functional correspondence between monkey and human brain areas. Nat Methods, 9: 277-282

Mantini D, Corbetta M, Romani GL, Orban GA, Vanduffel W (2013) Evolutionarily novel functional networks in the human brain? J Neurosci, 33: 3259-3275

McIntosh R, Gonzalez-Lima F (1994) Structural equation modeling and its application to network analysis in functional brain imaging. Hum Brain Mapp, 2: 2-22

Messé A, Rudrauf D, Benali H, Marrelec G (2014) Relating Structure and Function in the Human Brain: Relative Contributions of Anatomy, Stationary Dynamics, and Non-stationarities. PLoS Comput Biol, 10(3): e1003530

Mitra A, Snyder AZ, Tagliazucchi E, Laufs H, Raichle ME (2015) Propagated infra-slow intrinsic brain activity reorganizes across wake and slow wave sleep. Elife, 4: e10781

Spadone S, Della Penna S, Sestieri C, Betti V, Tosoni A, Perrucci MG, Romani GL, Corbetta M (2015) Dynamic reorganization of human resting-state networks during visuospatial attention. Proc Natl Acad Sci USA, 112: 8112-8117

Stephan KE, Harrison LM, Penny WD, Friston KJ (2004) Biophysical models of fMRI responses. Curr Opin Neurobiol, 14: 629-635

Sui J, Adali T, Pearlson GD, Calhoun VD (2009) An ICA-based method for the identification of optimal FMRI features and components using combined group-discriminative techniques. Neuroimage, 46: 73-86

Van Essen D, Anderson C, Felleman, D (1992) Information processing in the primate visual system: An integrated systems perspective. Science, 255: 419-423

Table 1 Names and abbreviations of the brain regions considered in the human connectome: from Hagmann et al. (2008) in alphabetical order. ROIs indexed from 1 to 33 concern the right hemisphere, those from 34 to 66 the left hemisphere (in reverse order of the left hemisphere).

Abbreviation	Brain region	ROI index
BSTS	**Bank of the superior temporal sulcus**	**12, 55**
CAC	**Caudal anterior cingulate cortex**	**23, 44**
CMF	**Caudal middle frontal cortex**	**17, 50**
CUN	**Cuneus**	**29, 38**
ENT	**Entorhinal cortex**	**1, 66**
FP	**Frontal pole**	**4, 63**
FUS	**Fusiform gyrus**	**5, 62**
IP	**Inferior parietal cortex**	**10, 57**
ISTC	**Isthmus of the cingulate cortex**	**31, 36**
IT	**Inferior temporal cortex**	**9, 58**
LING	**Lingual gyrus**	**27, 40**
LOCC	**Lateral occipital cortex**	**7, 60**
LOF	**Lateral orbitofrontal cortex**	**22, 45**
MOF	**Medial orbitofrontal cortex**	**26, 41**
MT	**Middle temporal cortex**	**13, 54**
PARC	**Paracentral lobule**	**30, 37**
PARH	**Parahippocampal cortex**	**2, 65**
PC	**Posterior cingulate cortex**	**33, 34**
PCAL	**Pericalcarine cortex**	**28, 39**
PCUN	**Precuneus**	**32, 35**
POPE	**Pars opercularis**	**18, 49**
PORB	**Pars orbitalis**	**21, 46**
PREC	**Precentral gyrus**	**16, 51**
PSTC	**Postcentra gyrus**	**15, 52**
PTRI	**Pars triangularis**	**19, 48**
RAC	**Rostral anterior cingulate cortex**	**24, 43**
RMF	**Rostral middle frontal cortex**	**20, 47**
SF	**Superior frontal cortex**	**25, 42**
SMAR	**Supramarginal gyrus**	**11, 56**
SP	**Superior parietal cortex**	**8, 59**
ST	**Superior temporal cortex**	**14, 53**
TP	**Temporal pole**	**3, 64**
TT	**Transverse temporal cortex.**	**6, 61**

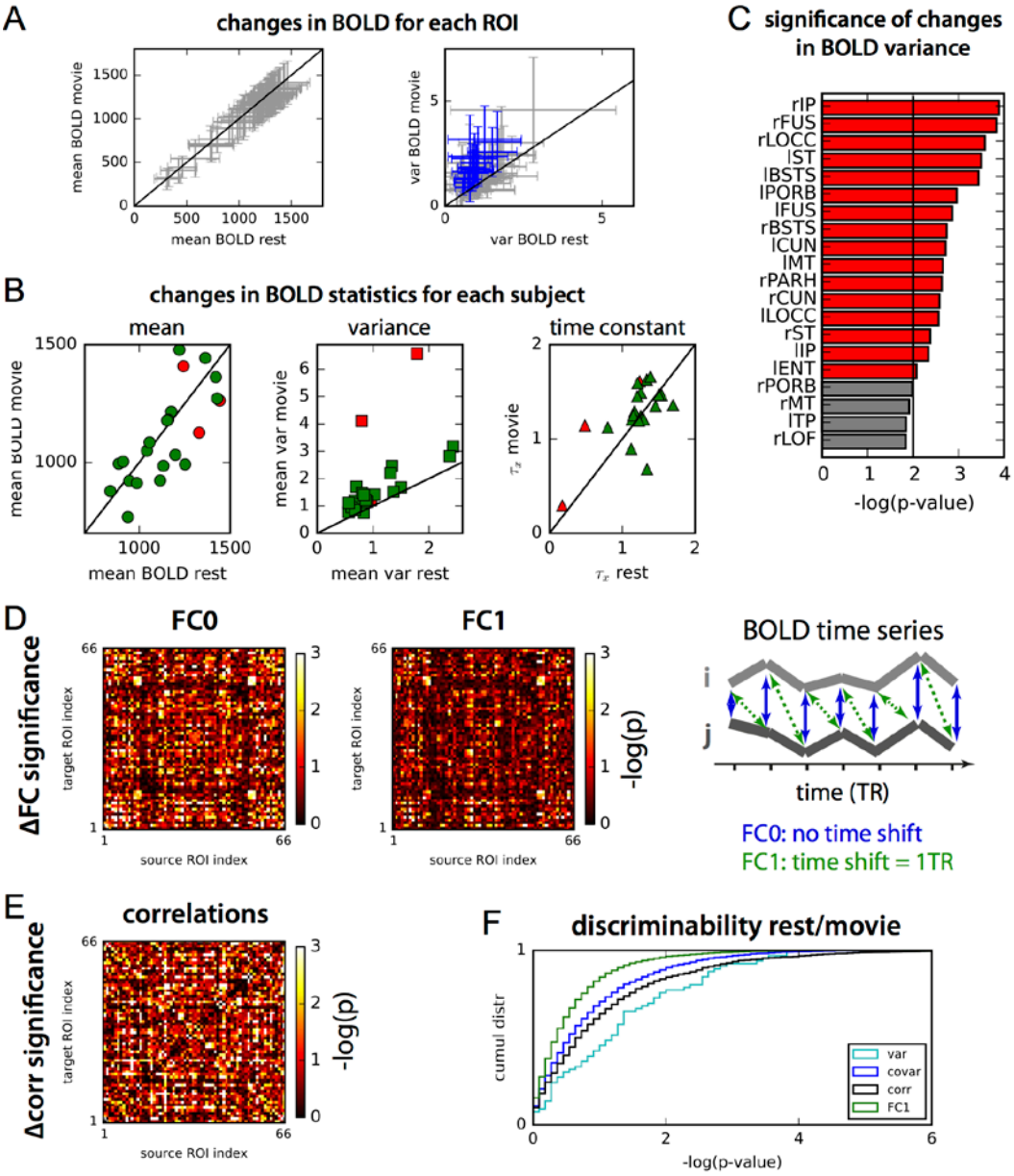

Fig. 1: fMRI data recorded on subjects watching a black screen (rest) or a movie. A: Changes in BOLD mean and variance between rest and movie conditions. Each cross represents one of the 66 cortical ROIs and the variability corresponds to the distribution over all 22 subjects. For the variances, blue crosses indicate significant changes between rest and movie (with p-value < 0.01). **B:** Comparison of BOLD means, variances and time constants τ_x for the two condition. Each symbol represents a subject, where the red symbols indicate the three discarded subjects, leaving 19 valid subjects for the following analysis. The black lines indicate identical values for rest and movie. **C:** Areas with most significant changes of BOLD variances between the two conditions. Significance is evaluated using Welch's t-test with unequal variances over valid subjects for each matrix element; 16 ROIs with p-values<0.01 (uncorrected), namely $-\log_{10}$(p-value)>2, are plotted in red. **D:** Significant changes in covariances matrices, FC0 with no time shift and FC1 with a time shift equal to 1 TR. The plotted score are $-\log_{10}$(p-value) as in C. **E:** Same as D for BOLD correlations instead of covariances. **F:** Comparison of cumulative distribution of p-values for variances (diagonal of FC0 in cyan), covariances (off-diagonal elements of FC0 in blue), correlations (black) and FC1 values (green).

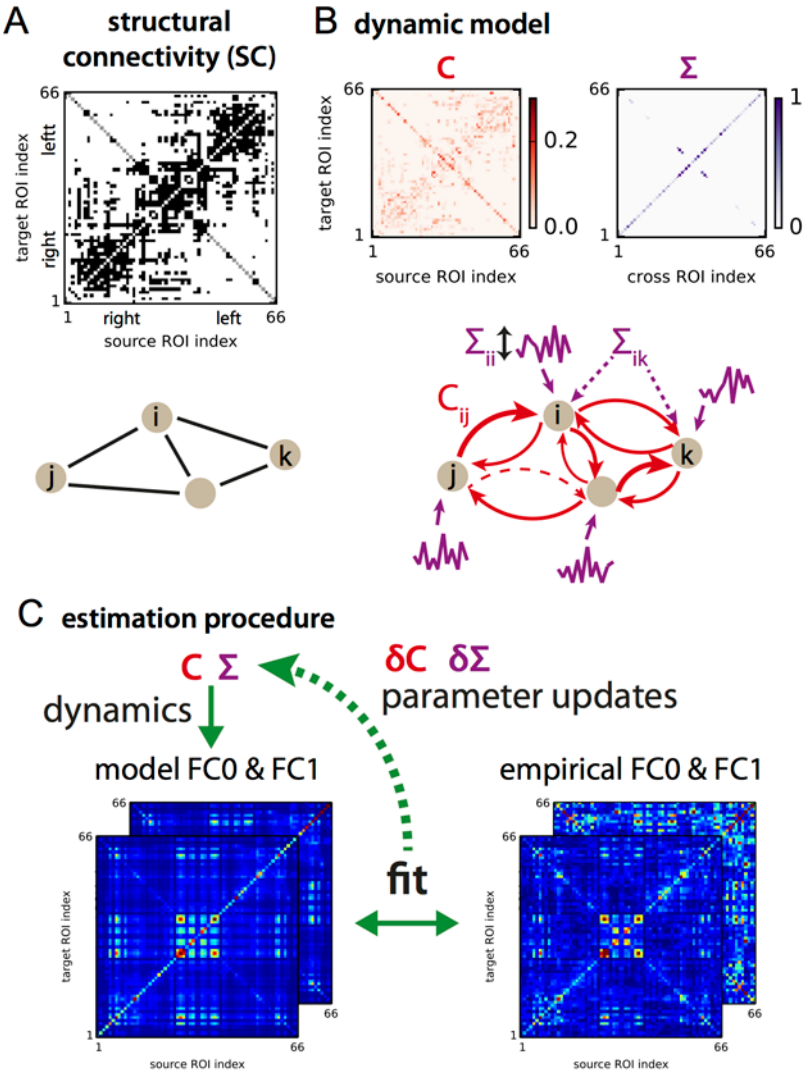

Fig. 2: Dynamic cortical model. A: DSI data provide the skeleton of the intracortical connectivity matrix. We add inter-hemispheric connections (gray pixels on anti-diagonal) as they are known to miss from DSI data. The formatting of all matrices in the present work shows the source and target ROIs on the x-axis and y-axis, respectively, as displayed here even though SC is symmetric. **B:** The parameters of the model are the recurrent connectivity C, that is EC, and the input covariances Σ (variances on the diagonal). Contrary to SC, EC is directed, as represented by the red arrows with various thicknesses for reciprocal connections. Some connections may also have zero weights (dashed arrow), equivalent to an absence of connections for the network dynamics. **C:** From the parameters, the model FC0 and FCτ matrices are calculated and compared to their empirical counterparts, which in turn gives the updates δC and $\delta\Sigma$ for the model. The optimization is performed until the minimal matrix distance is reached between the model and empirical FC matrices (average of both sets).

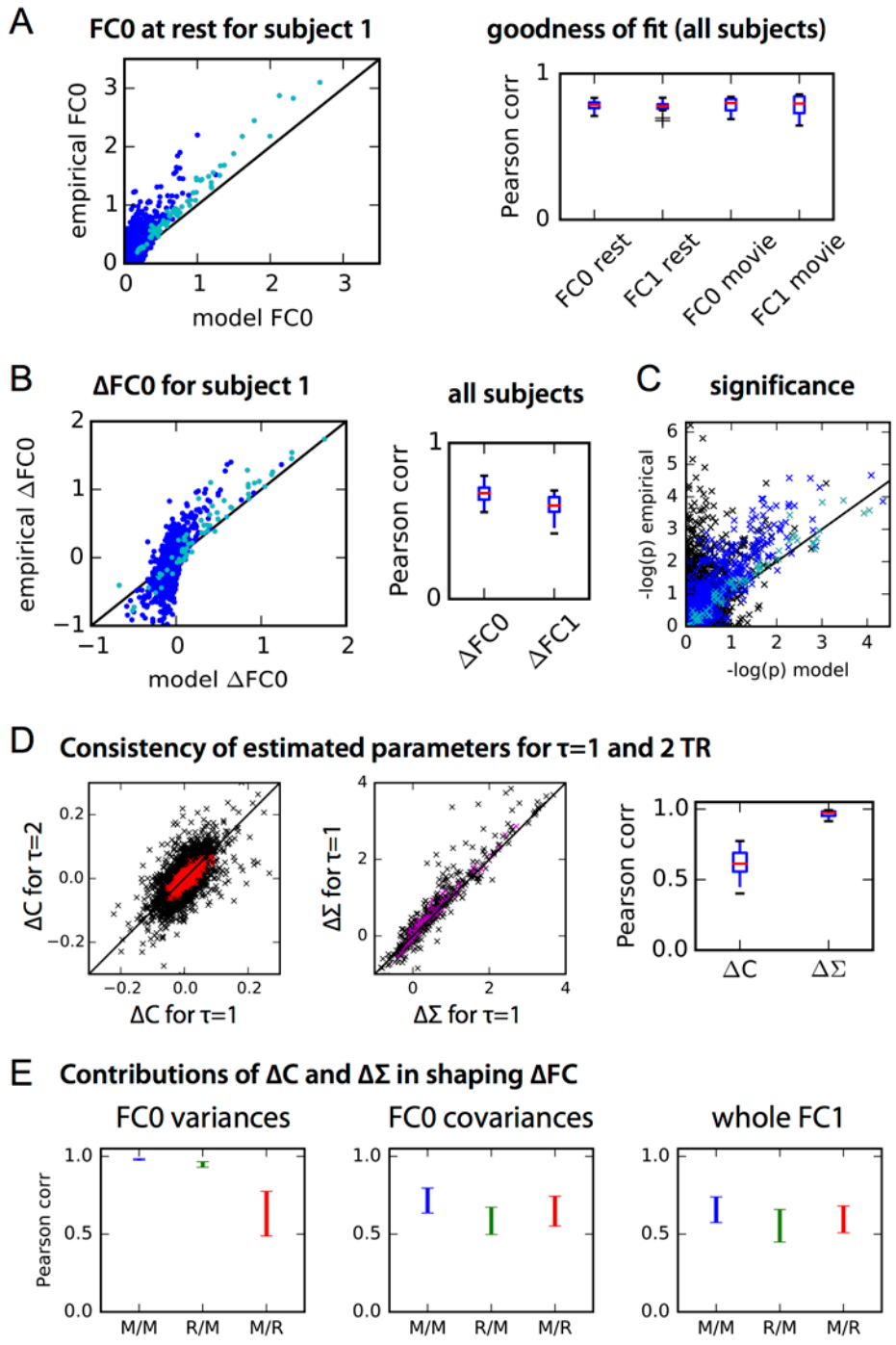

Fig. 3: Goodness of fit of the model. **A:** The left panel represents the model and empirical FC0 at rest for a single subject; each dot represent a matrix element (variances = diagonal elements in cyan, off-diagonal in dark blue). The right panel summarizes the goodness of fit as measured by the Pearson correlation coefficients for all subjects and the two conditions. **B:** Same as A for ΔFC0 and ΔFC1 (movie minus rest). **C:** Comparison of empirical and model p-values (uncorrected Welch's t-test) for the change in FC0 (from rest to movie). Cyan crosses indicate variances, blue indicate covariances corresponding to an existing connection in EC and black covariances for absent connections. **D:** Consistency between the ΔC and $\Delta \Sigma$ matrices obtained for each subject using two distinct optimizations, FC0/FC1 with τ=1 TR versus FC0/FC2 with τ=2 TRs. The left and middle panels show the correspondence of matrix elements, with the black diagonal indicating a perfect match. Mean values over all subjects are plotted in colors. The right panel displays

the Pearson correlation coefficients – one per subject – between the model estimates. **E:** Comparison of three models that combine the estimated C and Σ in the following manner: X/Y corresponds to C_X and Σ_Y with X and Y being either rest (R) or movie (M). The error bars correspond to the variability over the subjects of the Pearson correlation coefficients between the elements of FC matrices generated using C_X and Σ_Y and their empirical counterparts.

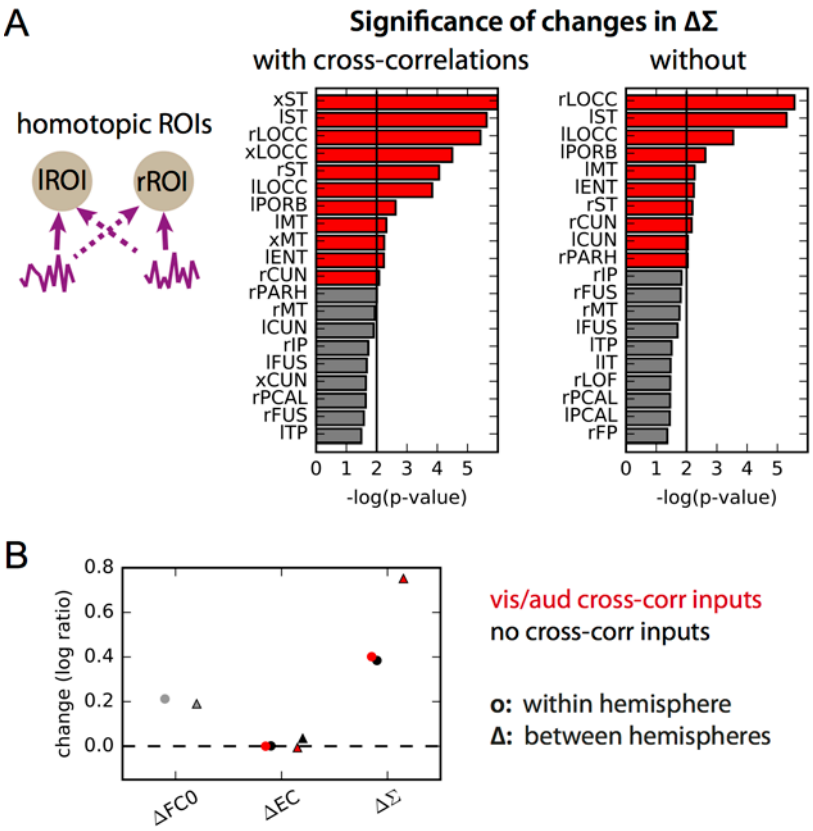

Fig. 4: Estimation of cross-correlated inputs. A: Σ elements with most significant changes for two models: one with cross-correlated inputs for visual and auditory ROIs (left), and one without (right). In addition to inputs to left and right ROIs, xROI indicates cross-correlated inputs, as indicated by dashed purple arrows on the left diagram. **B:** Comparison of the effect of the presence (red) or absence (black) of cross-correlated inputs on the parameters estimates. The circles indicate the change (log ratio of movie versus rest) for the summed within-hemisphere parameters, while triangles correspond to between-hemisphere parameters.

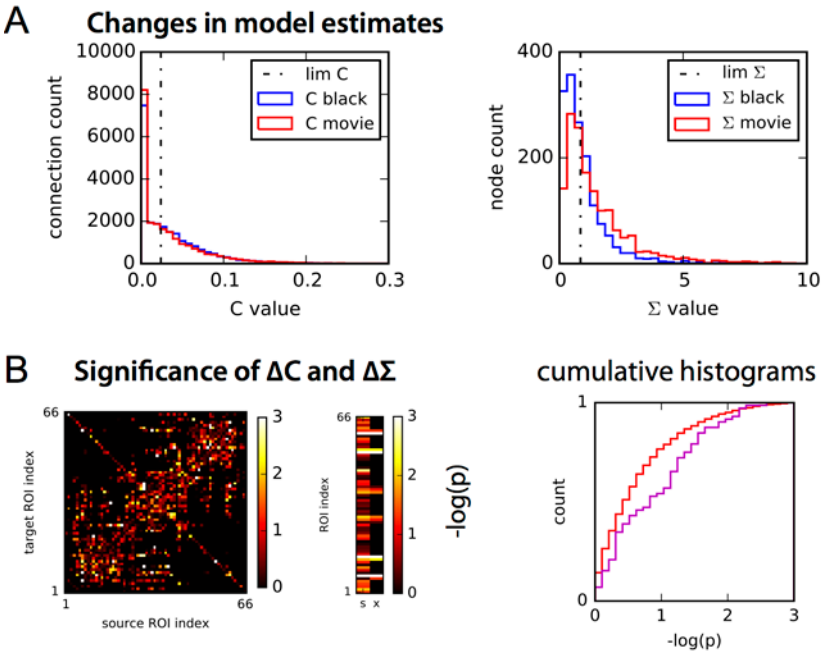

Fig. 5: Global changes in the estimated cortical connectivity *C* and input variances *Σ*. **A:** Histograms of *C* and *Σ* values in the two conditions. The median for each distribution of the rest condition is indicated in dashed-dotted line. **B:** Significance of the changes in C and *Σ* obtained from Welch's t-test (uncorrected). The plotted color corresponds to $-\log_{10}$(p-value), estimated with the same t-test between the two conditions as in Fig. 1 for FC. For *Σ*, the 7 cross-correlated inputs for visual and auditory ROIs are in the right column indicated by 'x', while the individual inputs to all ROIs are in the left column 's'. The right panel displays the cumulative distribution of p-values similar to Fig. 1F.

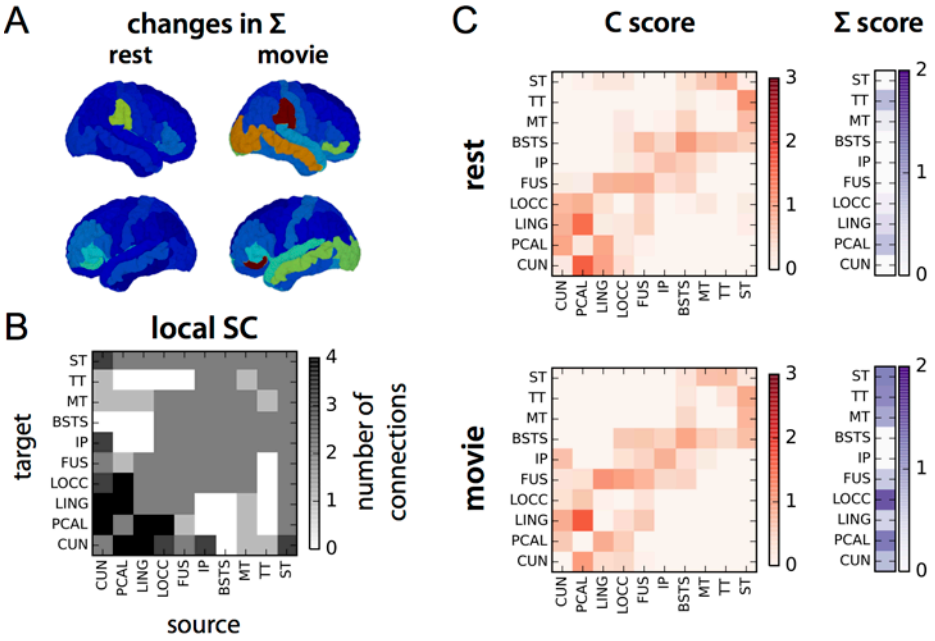

Fig. 6: Changes in the early visual and auditory pathways. A: Mean input variances Σ mapped on the cortical surface (left and right side views) for the two conditions; hot colors indicate large values. **B:** Structural connectivity between 14 ROIs in the early visual and auditory pathways, as well as 4 integration ROIs. Connections from the left and right hemispheres are grouped together. **C:** Statistical z-scores for the C and Σ values for the ROIs and connections in D for each condition (top and middle rows), as well as the score differences (bottom row). The scores measures – for each matrix element – the proportions of large values in the distribution in Fig. 5A, see Eq. (3).

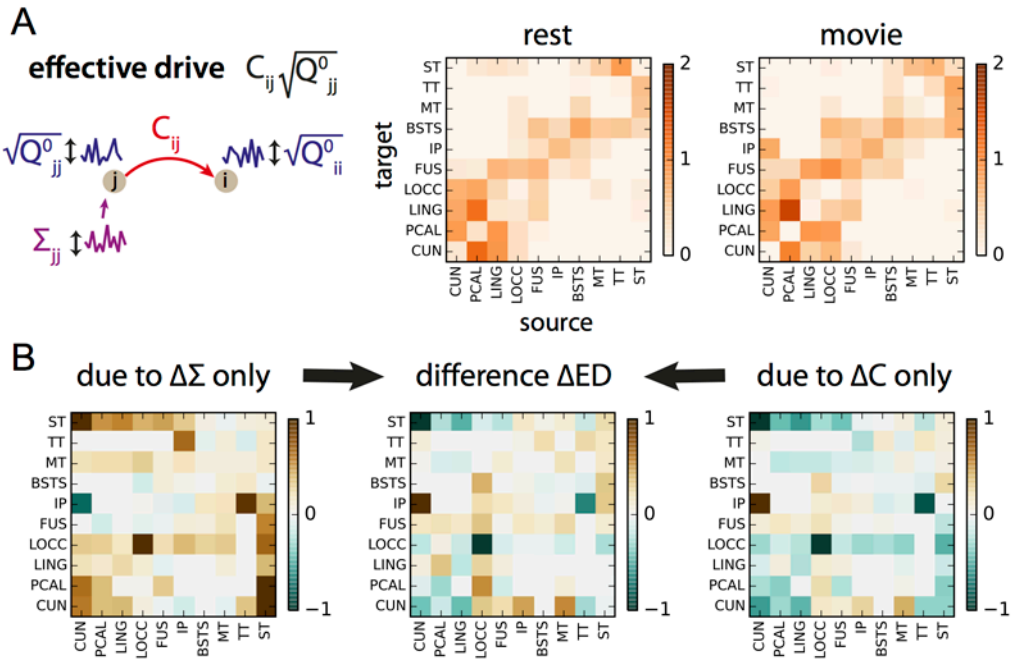

Fig. 7: Effective drive (ED) to quantify the information flow. A: Schematic representation of the propagation of fluctuations from ROI *j* to ROI *i*, with input variance Σ_{jj} (diagonal elements). The plotted values correspond to statistical scores as with C and Σ, taking into account the variability over subjects; see Eq. (4) for the formal definition. The concerned ROIs are the same as in Fig. 4D and E, namely the early visual and auditory pathways and three integration ROIs. **B:** Changes in effective drive for ROIs between rest and movie (middle panel), as well as contributions from ΔC (right) and $\Delta\Sigma$ (left).

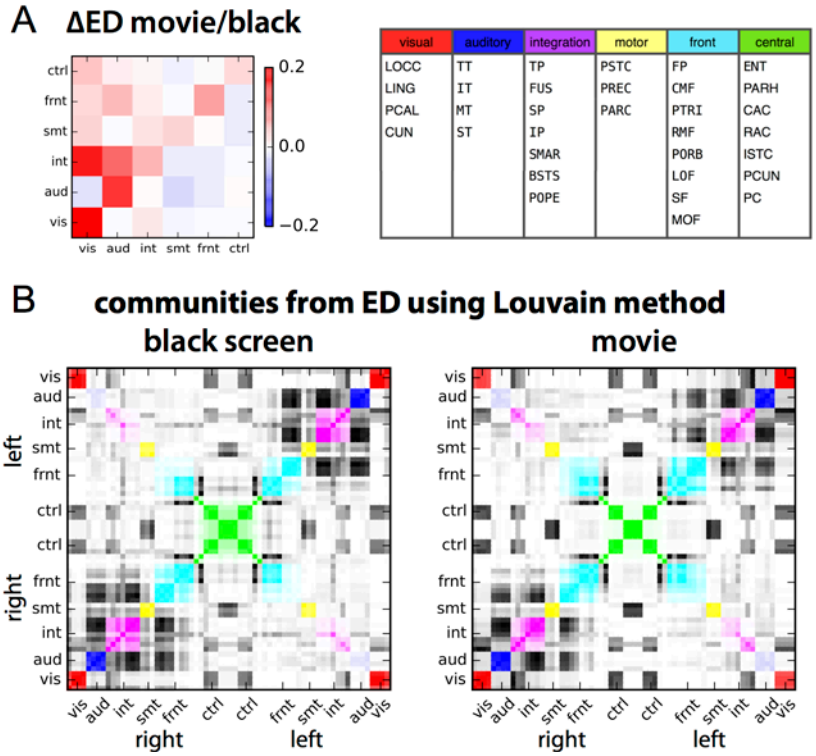

Fig. 8: Path selection and inter-hemispheric integration in the cortex. A: Changes in effective drive between ROIs pooled in 6 groups: visual in red, auditory in dark blue, integration in purple, motor in yellow, frontal in cyan and "central" in green. The change is calculated in % of the value for rest. The lists of the group concern ROIs from both hemispheres. **B:** Communities estimated using the Louvain method from the effective drive in Fig. 7 for each of the two conditions. The plotted values correspond to averages over the subjects, for each of which the Louvain method was applied 10 times on the ED matrix. The connections within the groups are displayed in color. ROIs are ordered to show the left and right hemispheres separately.